

The Effects of Processing Parameters on Defect Regularity in Ti-6Al-4V Parts Fabricated By Selective Laser Melting and Electron Beam Melting

Haijun Gong*, Khalid Rafi*, Thomas Starr†, Brent Stucker*

*Department of Industrial Engineering, †Department of Chemical Engineering,
J. B. Speed School of Engineering, University of Louisville, Louisville, KY 40292

Accepted August 16th 2013

Abstract

Processing parameter has an important effect on Selective Laser Melting (SLM) and Electron Beam Melting (EBM) processes. Defects are easily formed by deviating from optimized processing parameters. This study purposely fabricated Ti-6Al-4V specimens with defects by varying process parameters from the factory default settings in both SLM and EBM equipment. Specimen's density was measured based on the Archimedes method for estimating porosity. Microscopy of specimen's top surface were observed to compare melt pool and overlap. "Marginal Parameters" is identified to describe the processing parameters which are capable of fabricating specimens with certain porosity. As a result, a correlation between defect regularity and marginal parameters has been established. The effect of marginal parameters on the melt pool is discussed to explain defect formation.

1. Introduction

Metal powder bed fusion based Additive Manufacturing (AM) processes, such as Selective Laser Melting (SLM) and Electron Beam Melting (EBM), are successfully being used to manufacture parts from metallic materials including stainless steel, maraging steel, cobalt chromium, titanium alloys and more. In particular, additively manufactured Ti-6Al-4V parts are of wide interest for aerospace, biomedical and industrial fields due to its fracture resistance, fatigue behavior, corrosion resistance and biocompatibility [1].

An SLM machine selectively melts metallic powder layers, forming a solid part on a building plate. Inside an SLM build chamber, there is a material dispenser platform along with a recoating unit used to feed new powder over the build platform, as shown in Fig. 1. Parts are then built up additively, layer by layer, based upon a sliced CAD representation of the desired part.

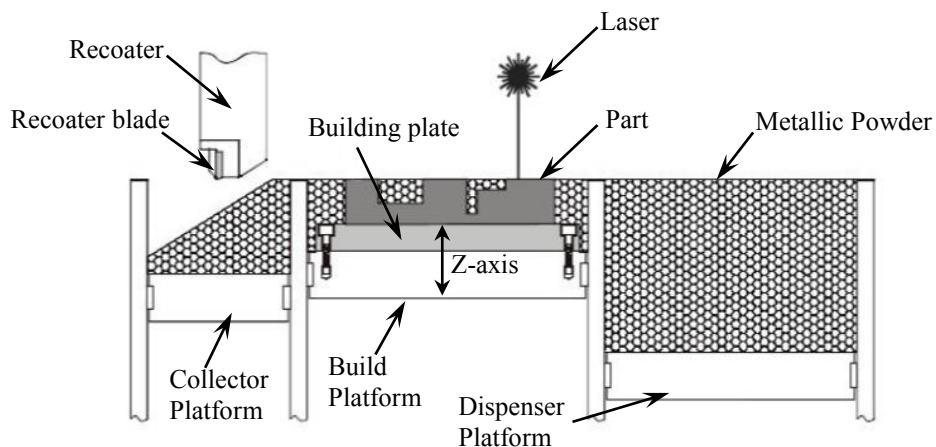


Fig. 1 Schematic of SLM Process

In the EBM process, instead of a laser beam, an electron beam is generated via a tungsten filament in an electron gun, as shown in Fig. 2. The powder bed is first pre-heated using a defocused electron beam in order to enhance the conductivity and cohesion of particles, and to avoid powder spreading in the chamber. The microstructural characteristics of EBM-built material are also influenced by the pre-heating process. A more concentrated beam of electrons is then used to melt the metal powder according to the proscribed CAD data. When the electrons penetrate the powder surface and into the powder grains, their velocity is slowed. By doing this, their kinetic energy is converted into thermal energy and the metal powder reaches its melting temperature [2]. Electromagnetic lenses are used to control the electron beam, in contrast to the scanning galvanometers used in SLM.

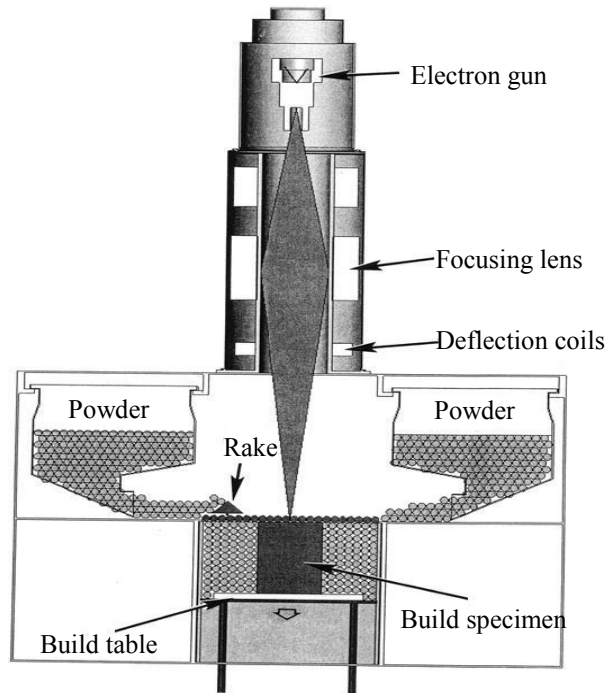


Fig. 2 Schematic of EBM Process

In recent years, SLM and EBM of Ti-6Al-4V have made significant progress [3-6], especially related to optimization of processing parameters and characterization of Ti-6Al-4V materials. However, many authors indicated that SLM and EBM-built materials are subject to porosity inclusion, which influences mechanical properties [7, 8]. In order to explain defect generation, this study carried out experiments with various processing parameter combinations. For clarity, a number of non-optimal parameter combinations were named “marginal parameters”. The effect of marginal parameters on the variation of melt pool and hatch overlap is discussed by comparing the top surface of specimens.

2. Ti-6Al-4V powder properties

In this study, Raymor Ti-6Al-4V powder was used in the SLM process. Currently, no literature reports on the optimized processing parameters for this specific fine powder, compared to EOS-provided powder. Fine powder is not suitable for the EBM process because small particles will be easily influenced by electrostatic charge, which results in serious powder spreading above

the building platform [9]. Therefore, Arcam Titanium Ti-6Al-4V powder was used for the EBM process.

2.1 Raymor Ti-6Al-4V powder for SLM

Raymor Ti-6Al-4V (Grade 23) powder has an apparent density of 2.55 g/cm³. Most particles have diameter no more than 45 μm (0-25 μm, 34.1%; 25-45, μm 63.1%; +45 μm, 2.8%). Fig. 3 shows the powder morphology under a Scanning Electron Microscope (SEM). The powder was measured using a Microtrac S3000 laser-based particle size analyzer. The spherical particles have a size distribution between 17.36 μm (D₁₀) and 44.31 μm (D₉₀) with Mean Volume Diameter around 30 μm. Its particle size is nearly normally distributed around two peaks, with diameter 5.46 μm and 28.67 μm. Raymor Ti-6Al-4V powder contains a lot of fine particles, compared to EOS Titanium Ti-6Al-4V powder [10].

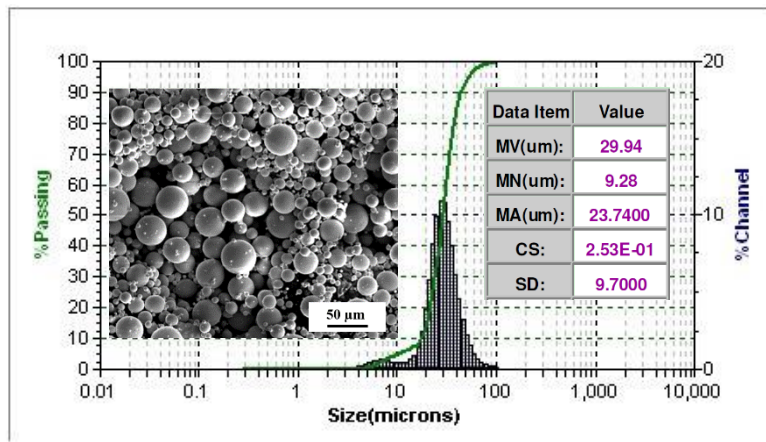


Fig. 3 Raymor Ti-6Al-4V Powder Morphology and Particle Size Distribution

2.2 Arcam Ti-6Al-4V powder for EBM

Arcam Titanium Ti-6Al-4V ELI powder has a spherical morphology, with apparent density no more than 2.7 g/cm³. The particle size analysis showed that Arcam powder has a size distribution between 46.94 μm (D₁₀) and 99.17 μm (D₉₀) with Mean Volume Diameter around 72.69 μm. The particle size is nearly normally distributed. But it has a small percentage of particles with diameter larger than 100 μm, as shown in Fig. 4.

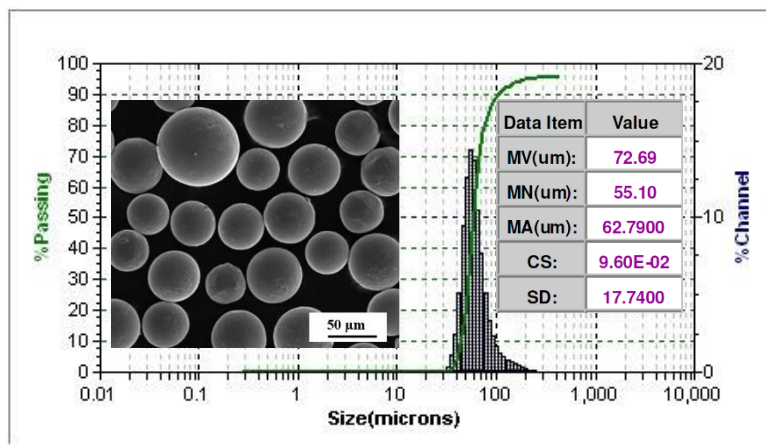


Fig. 4 Arcam Ti-6Al-4V Powder Morphology and Particle Size Distribution

3. Design of Experiments

Energy density is usually used to describe the average applied energy per volume of material during a powder bed fusion process. Significant processing parameters are included in an energy density equation. For example, energy density can be expressed by equation (1) for the SLM process [11].

$$E = \frac{P}{v \cdot h \cdot t} \quad (1)$$

where P is laser power, v is scanning speed, h is hatch spacing and t is layer thickness. Generally, these parameters have a complicated mutual effect during the laser melting process when all of parameters are varied in an experiment. The melt pool variation and defect generation will be easily characterized if some parameters are kept constant. According to the equation (1), it is noted that laser power and scanning speed have an inverse impact on the energy density. So this experiment adopted a factorial design based on these two parameters in order to correlate the energy density and defect regularity. An EOS M270 Direct Metal Laser Sintering (DMLS) system was utilized to fabricate specimens. The experimental factors and levels are given in Table 1.

Table 1 Factors and Levels of Factorial Experiment (SLM: Ti-6Al-4V)

Factor	Level
Laser Power (W)	40, 80, 120, 160
Scanning Speed (mm/s)	120, 240, 360, ..., 1560
Hatch Spacing (μm)	100
Layer Thickness (μm)	30

For the EBM process, “energy density” can also be expressed similarly as equation (1), by substituting electron beam power for laser power [9]. An Arcam S400 EBM system was used for this study. However, the scanning speed cannot be directly varied in the Arcam system. It is dynamically controlled through a “speed function” during the melting process in order to achieve the correct melt pool size. The speed function is related to the “max current” and “speed function index”. Additionally, “line offset” and “focus offset” are also influential processing parameters to the EBM process. Therefore, this study utilized max current, line offset, focus offset, and speed function index as the primary experimental factors. As shown in Table 2, three levels for each factor were selected for studying their significance on the defects through a Taguchi experiment (L9). The One-Factor-at-A-Time (OFAT) method was also employed to further investigate the significant factors.

Table 2 Factors and Levels of Taguchi Experiment (EBM: Ti-6Al-4V)

Factor	Level
Max Current (mA)	10, 20, 30
Line Offset (mm)	0.15, 0.20, 0.25
Focus Offset (mA)	5, 10, 15
Speed Function Index	60, 120, 180

After SLM and EBM specimens were built, each specimen’s density was measured using the Archimedes method [12] according to ASTM B962-08. The measured density was compared with the nominal density of the Ti-6Al-4V material to estimate porosity according to equation (2),

$$R_D = 1 - \frac{\rho_e}{\rho_n} \quad (2)$$

where R_D is porosity, ρ_e is measured density, and ρ_n is nominal density. It can be seen that, the lower the measured density, the larger the porosity.

4. Results and Discussion

In this section, the cause of defect generation during SLM and EBM processing is analyzed and compared. Processing parameters are further classified based on their effect on the porosity generation. Microscopy of specimen's top surface illustrates the change of melt pool and overlap between hatch lines.

4.1 Effect of Processing Parameters on SLM Ti-6Al-4V

4.1.1 Porosity Distribution and ANOVA

Fig. 5 shows the porosity of SLM produced Ti-6Al-4V specimens with uncertainty value. From Fig. 5(a), it can be seen that there is no apparent porosity when scanning speed is between 600 mm/s and 1600 mm/s at a laser power of 160 W. When the scanning speed is less than 600 mm/s, which is a higher energy density, the increased porosity implies internal defects in the specimens. Moreover, porosity is not available when the scanning speed is decreased below 360 mm/s, because specimens were not successfully built. The deposited layer was seriously deformed resulting in crash with the recoating blade. When laser power is at 120 W in Fig. 5(b), slow scanning speed (<360 mm/s) also causes build failure. There could be no porosity or internal defects, when the scanning speed ranges from 720 to 1200 mm/s. After that, the reduced energy density generates insufficient melting temperature in the Ti-6Al-4V powder, and the porosity increased with the scanning speed.

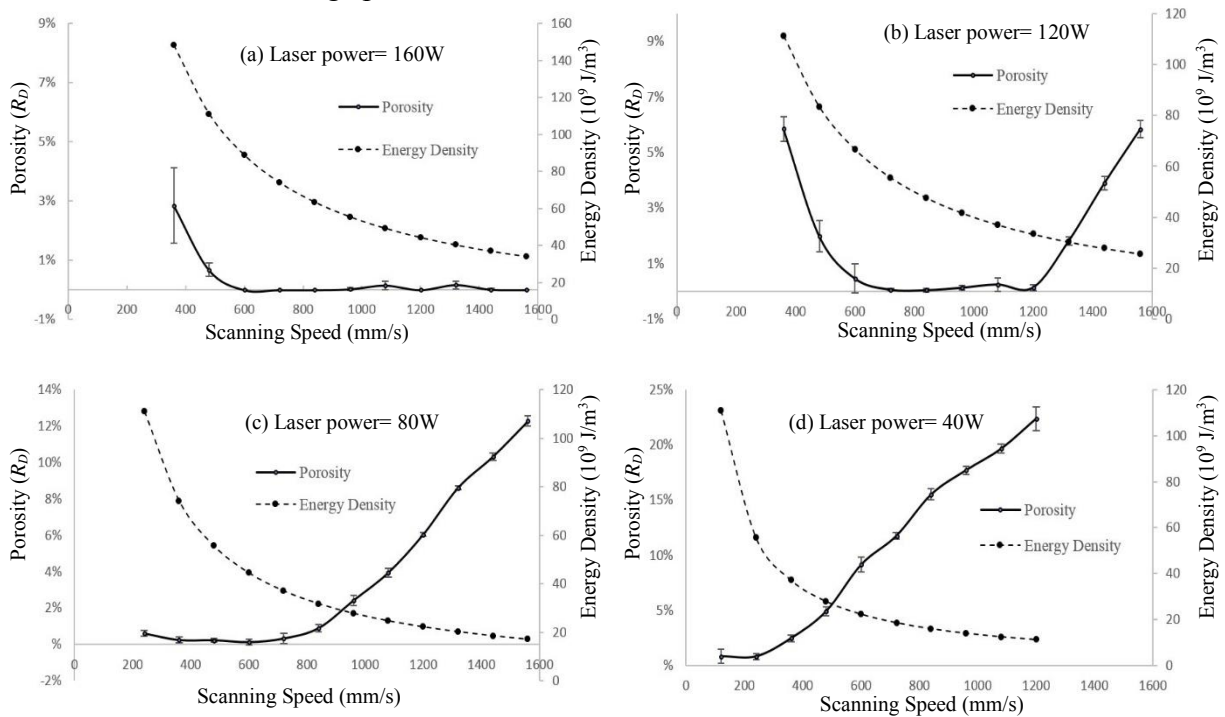


Fig. 5 Porosity of SLM-Produced Ti-6Al-4V Specimen

If the laser power is reduced to 80 W, a porosity free specimen is only available when the scanning speed is around 600 mm/s, as shown in Fig. 5(c). Lowering the scanning speed leads to a small porosity. But the porosity is dramatically increased when increasing the scanning speed. When the laser power is lowered to 40 W, all specimens are assumed to contain defects even if at a slow scanning speed. At 1200 mm/s, the specimen's porosity is even higher than 20%, as shown in Fig. 5(d).

ANOVA of factorial experiment is summarized in Table 3. It can be seen that the F values of both laser power and scanning speed are larger than the threshold ($F_{0.05, 3, 160}$ and $F_{0.05, 12, 160}$) which indicate significance with 95% confidence level. This conforms to the results of other references with respect to SLM.

Table 3 ANOVA of Factorial Experiment

Source	Degree of freedom	Sums of Squares (SS)	Adj. Sums of Squares (SS)	Adj. Mean Square (MS)	F value
Laser Power	3	0.25	0.35	0.12	99.26
Scanning Speed	12	0.16	0.16	0.01	11.27
Error	160	0.19	0.19	0.00	
Total	175	0.60			

$F_{0.05, 3, 160}=2.66$; $F_{0.05, 12, 160}=1.81$

4.1.2 Process Window and Marginal Parameters

According to the porosity distribution, a process window can be introduced to show the effect of laser powers and scanning speeds on defects when laser melting Raymor Ti-6Al-4V powder. SLM processing parameters are classified into “fully dense parameters” (Zone I), “over melting parameters” (Zone II), “incomplete melting parameters” (Zone III), and “over heating parameters” (Zone OH), as shown in Fig. 6. The energy density of each point in the process window could be simply represented by slope of a line between the origin and a point on the graph, if the hatch spacing and layer thickness are constant. For example, all points along the dash line in Fig. 6 have the same energy density. The higher the slope value, the larger the energy density.

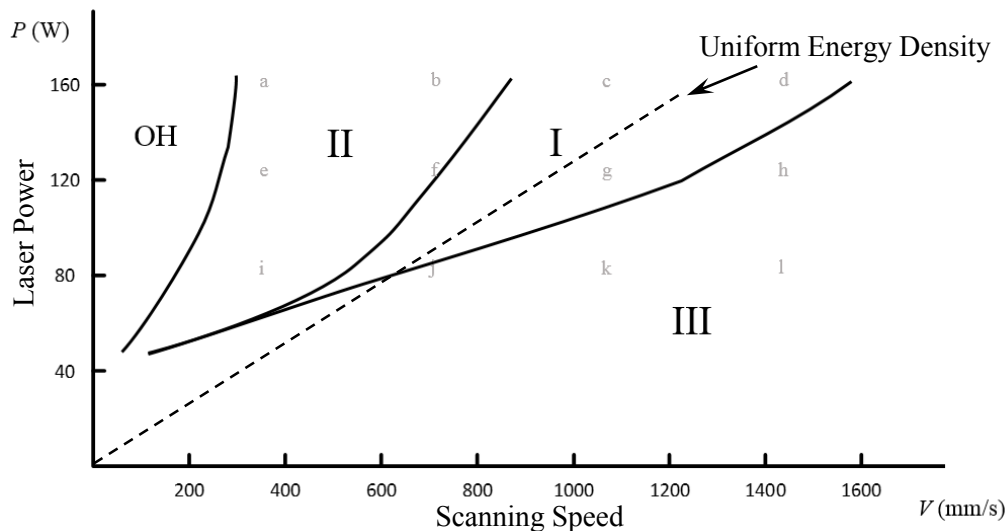


Fig. 6 Process Window for SLM Raymor Ti-6Al-4V Powder

The Zone I parameters are capable of building fully dense specimens with Raymor Ti-6Al-4V powder. It is notable that energy density should be sufficient to avoid incomplete melting. In addition, even if the energy density meets the minimum requirement, porosity could also be included in the specimen. For example, the lower portion of the dashed line in Fig. 6 demonstrates that these laser power and scanning speed cannot be used to fabricate porosity free specimen. Specimens may not be built using Zone OH parameters. Because laser irradiation produces a large quantity of heat which is unable to be conducted away from the specimen immediately. The accumulated strain energy results in serious deformation causing collision with the recoating unit.

Zone II and III parameters can be used to fabricate Ti-6Al-4V specimens with porosity. These parameters are known as “marginal parameters” in this study because they are distributed to the margins of Zone I. It is a straightforward situation that insufficient energy density causes smaller melt pools and partially molten powder in Zone III. Thus, voids among powder particles are entrapped under the solidified hatch lines so that the overall density of the specimen is lowered. However, defects also exist in the specimens fabricated by the Zone II parameters. This implies that extra energy not only causes microscopic structural rearrangements of SLM Ti-6Al-4V, but also a complex transport phenomenon of macroscopic masses over macroscopic distances, with ablation and compression of material and with large internal energies compared to chemical activation energies [13].

In order to analyze the melting process under different processing parameters, typical solidified top surface were observed under SEM, as shown in Fig. 7. Each picture corresponds to the processing parameter combination specified in Fig. 6.

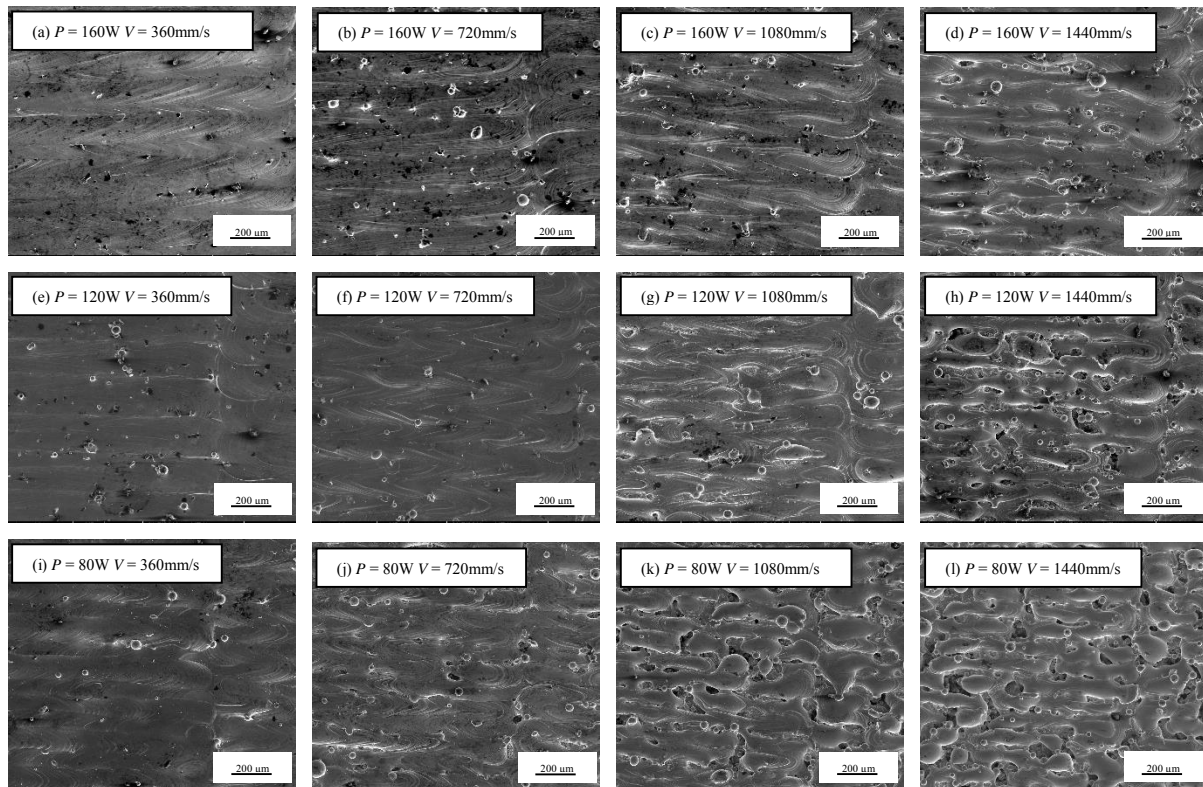


Fig. 7 Scanning Electron Microscopy of Top Surface of Laser Melted Ti-6Al-4V

In Zone I, the processing parameters are able to build fully dense specimens. Fig. 7 (c), (d), (f) and (g) show the solidified hatch lines of these specimens. With increasing the scanning speed, the melt pool size is gradually reduced. Because hatch spacing is constant, the reduced melt pool size results in decreased overlap, which deteriorates the top surface's roughness, as shown in Fig. 7 (d) and (g). Although voids occasionally appear due to discontinuous hatch lines, they are eliminated by the following recoating and melting process. Thus, no apparent porosity was detectable in the specimens through Archimedes method and destructive characterization techniques. Fig 7 (a), (b), (e) and (i) show the top surface melted by the Zone II marginal parameters. The melt pool was extremely extended with high energy density, especially in the ends of each hatch line due to the ramping phenomenon of scanning speed. On the other hand, energy deficiency causes the melting discontinuity when using the Zone III marginal parameters. As shown in Fig. 7 (h), (j), (k) and (l), many breaking spots are visible along the hatch lines.

4.1.3 Defects Caused by Zone II Marginal Parameters

A large melt pool results in the increased overlap between hatch lines. However, it can be seen that the highly overlapped hatch lines do not necessarily form voids or defects on the remelted top surface. A certain amount of spherical particles and pits are observable on a solidified top surface, as shown in Fig. 8. It is believed that the porosity of specimens built by the Zone II marginal parameters is directly correlated with these particles and pits. When melting the Ti-6Al-4V powder at higher energy density, laser irradiation not only causes larger melt pool, but also extra heat which evaporates the molten materials. The melt pool is subject to recoil force from the evolving vapor, which ejects molten materials [14]. This mechanism is similar to the ablating process of laser drilling. But the materials are even more easily extracted from a powder bed.

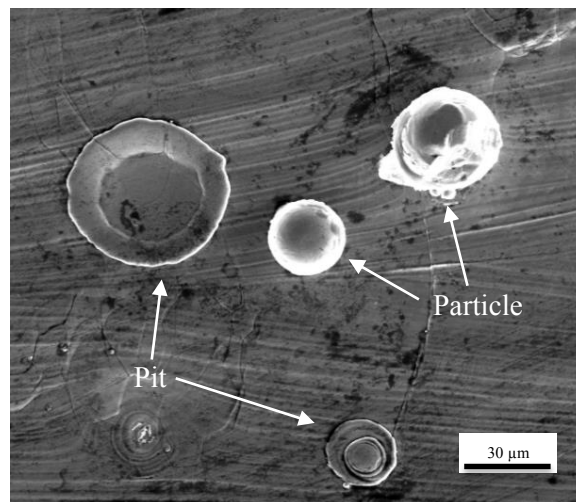


Fig. 8 Scanning Electron Microscopy of Pits and Particles on Top Surface of SLM Specimen

The molten metal rapidly solidifies above the building platform and forms spherical particles, some of which fall down and are then welded together with the top surface of the specimens. Small welded particles will be melted together with recoated powder particles. However, large particles, which attach to the top surface, will be easily touched and removed by the recoating blade, as shown in Fig. 9. Pits will be formed with a hollow spherical crown shape after removal. Large pits could be filled with recoated powder. But small pits could be easily entrapped underneath new layers as defects. Due to their occasional formation, these defects are

distributed stochastically in the specimen, instead of directly being correlated with processing parameters. This explains why the uncertainty value of specimen porosity built by the Zone II marginal parameters is larger than that by the Zone III marginal parameters.

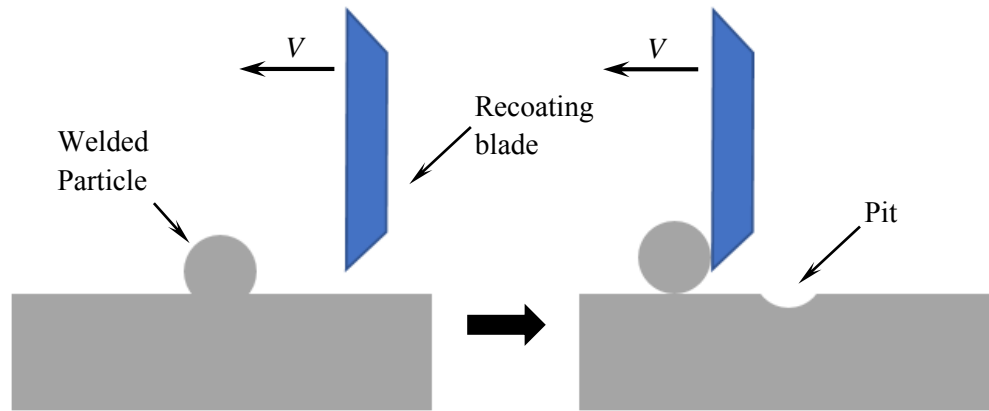
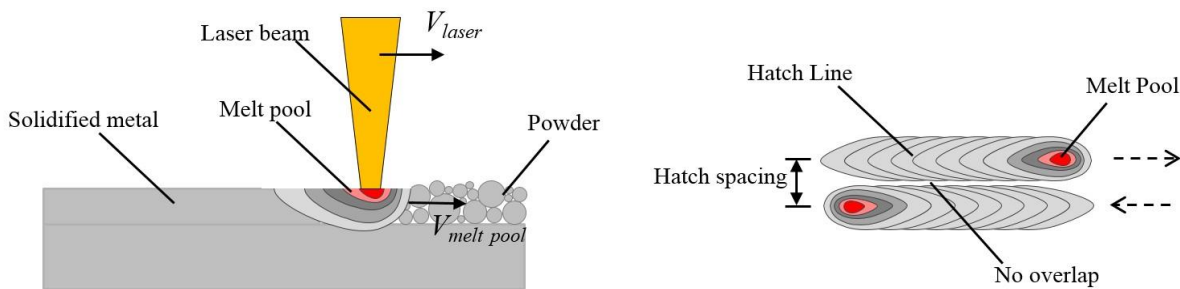


Fig. 9 Schematic of Defect Caused by Recoating during SLM Process

4.1.4 Defects Caused by Zone III Marginal Parameters

The discontinuity of hatch lines results from the velocity inequality between laser scanning speed and melt pool interface motion. When laser power is applied to the powder bed, the powder particles form a melt pool in a transient process. Temperature of the interface between the molten material and un-melted powder is around the melting point (1660 °C for Ti-6Al-4V). If there is not enough energy furnished to the interface to preserve melting and steady melt pool, the velocity of the interface will be occasionally slower than that of the laser spot motion (i.e. $V_{melt\ pool} < V_{laser}$), as illustrated in Fig. 10 (a). Thus, hatch lines can hardly be formed continuously. Moreover, due to the reduced melt pool size, the overlap between two hatch lines is very limited, which exacerbates the wetting condition for the following layer. If the molten material fails to wet on the previous layer and adjacent hatch line (Fig. 10 (b)), it will easily accumulate to form a rounded surface due to surface tension. Therefore, the voids or pores are seriously generated.



(a) Laser melting metallic powder (b) Top view of two adjacent hatch lines
 Fig. 10 Schematic of Defect Caused by Zone III Marginal Parameters of SLM Process

A typical solidified surface is shown in Fig. 11, which was fabricated by the Zone III marginal parameters. The scanning direction is indicated in the figure. Some powder particles were sintered on the top surface which are visible through the voids. The voids are randomly distributed with irregular morphology along and between hatch lines.

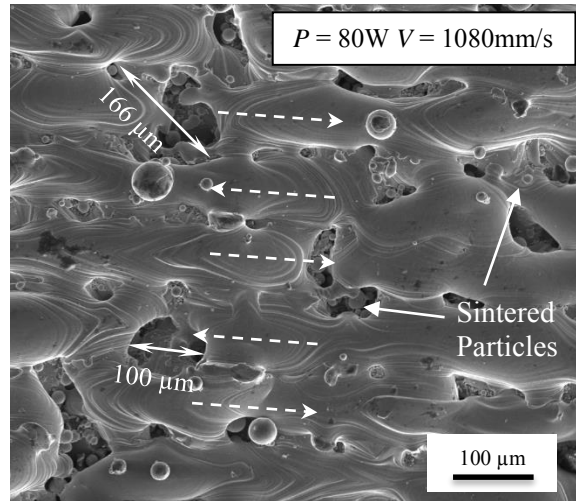


Fig. 11 Top Surface Fabricated by Zone III Marginal Parameters of SLM Process

4.2 Effect of Processing Parameters on EBM Ti-6Al-4V

4.2.1 Mean Porosity Distribution and ANOVA

EBM specimens' mean porosity versus individual experimental factor is shown in Fig 12. The porosity for each level of a particular factor corresponds to an average of three experimental runs at that level, typically with four replicates, representing an average of 12 density measurements.

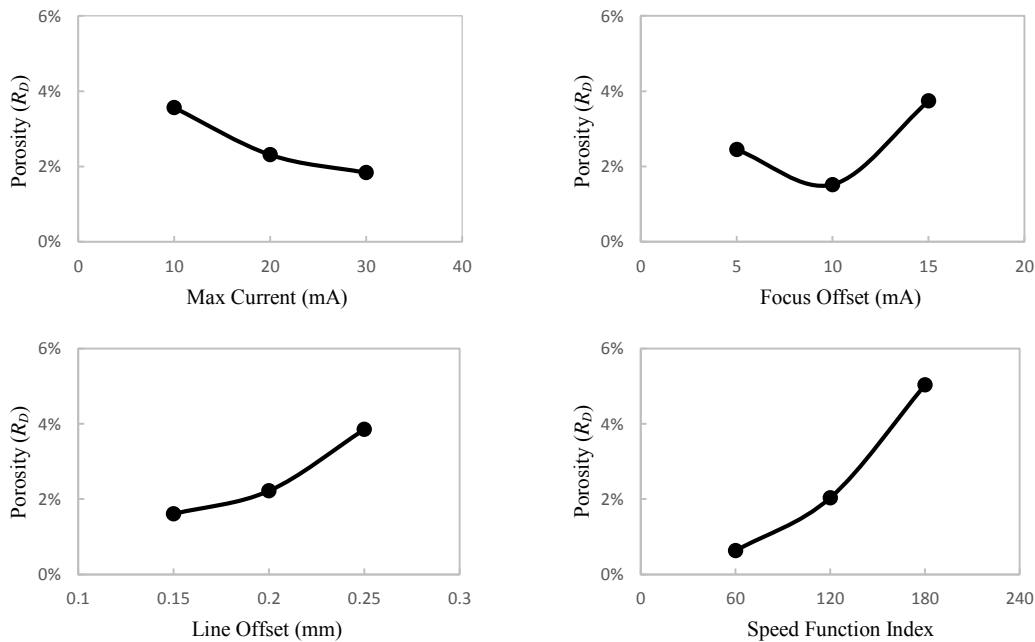


Fig. 12 Mean Porosity at Each Level of Taguchi Experimental Factors

ANOVA was also performed to statistically evaluate the effect of each parameter on porosity of EBM Ti-6Al-4V specimens. The results of ANOVA are summarized in Table 4. It can be seen that all F values are larger than $F_{0.05, 2, 27}$. Thus, all experimental parameters could be considered as significant factors influencing the porosity (95% confidence level). The speed

function number has the most significant influence on specimens' porosity, followed by line offset, focus offset, and max current.

Table 4 ANOVA of Taguchi Experiment

Source	Degree of freedom	Sums of Squares (SS)	Mean Square (MS)	F value
Max Current	2	0.04	0.02	58.94
Focus Offset	2	0.06	0.03	93.14
Line Offset	2	0.06	0.03	102.02
Speed Func. No.	2	0.23	0.12	376.73
Error	27	0.01	0.00	
Total	35	0.40		

$F_{0.05, 2, 27}=3.35$

However, it is difficult to correlate the speed function index with actual energy input based on the existing references. Thus, line offset, focus offset and max current were studied by using OFAT method with a constant speed function index (default 98 for EBM Ti-6Al-4V powder) at layer thickness 50 μm . The OFAT experiments also illustrate the significance of line offset and focus offset to porosity change. Based on the porosity distribution, the increased line offset and focus offset could also be considered marginal parameters. Otherwise, there is no apparent porosity fabricated by varying max current. It is assumed that the Arcam system is able to regulate the scanning speed automatically according to the powder bed temperature, even at the reduced beam current. Thus, analysis and discussion about EBM processing parameters are mainly focused on line offset and focus offset.

4.2.2 Defects Caused by the Increased Line Offset

Porosity distribution versus line offset is shown in Fig. 13. It can be seen that the porosity is increased by increasing line offset, especially when the line offset is larger than 0.18mm.

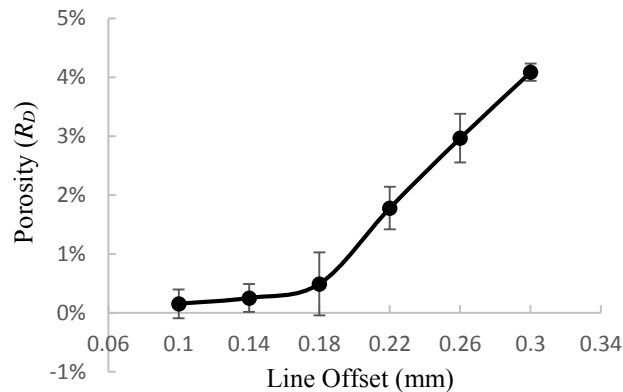


Fig. 13 Porosity versus Line Offset

Line offset refers to the distance between two hatch lines, similar to hatch spacing in SLM. According to the energy density equation, increased line offset will reduce the energy density value. The OFAT experimental result indicates that porosity is dramatically increased when the line offset value is larger than 0.18mm. In order to correlate line offset with defect generation, solidified hatch lines are shown in Fig. 14.

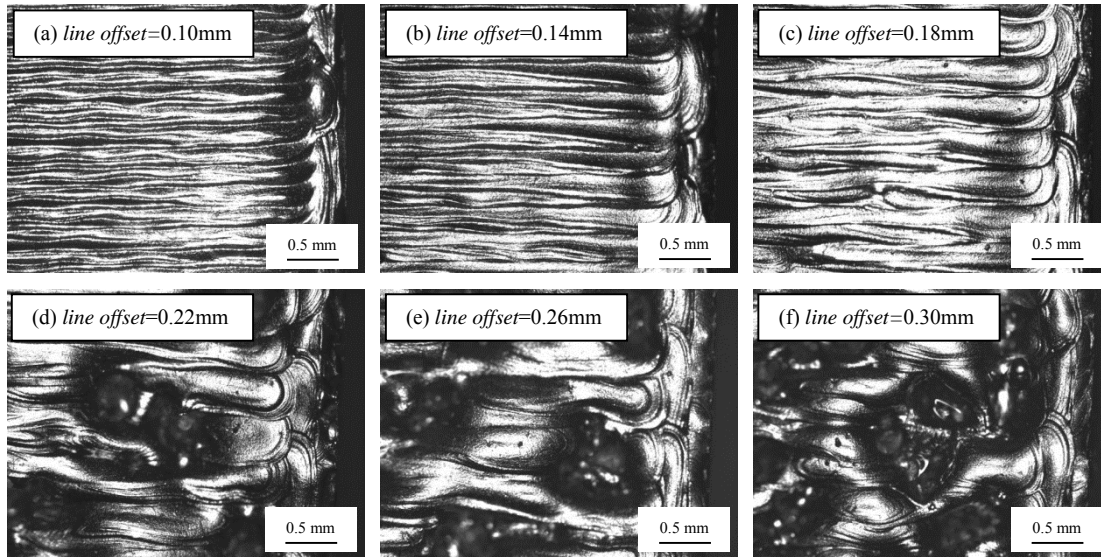


Fig. 14 Solidified Top Surfaces of EBM Specimens by Varying Line Offset

When line offset is 0.1mm (default value), the solidified hatch lines are arranged equally. No apparent pores or defects are formed between hatch lines. However, overlap between hatch lines will be reduced if the line offset is increased to 0.14 and 0.18mm. Although there are no visible pores or voids on the top surface (Fig. 14 (b) and (c)), a small amount of porosity is detectable from the porosity curve shown in Fig. 7. This could be attributed to the un-melted powder under the adjacent hatch lines, as shown in Fig. 15. The powder gap was trapped inside the specimen as defects. This means not all powder is melted during the EBM process if the line offset value is increased.

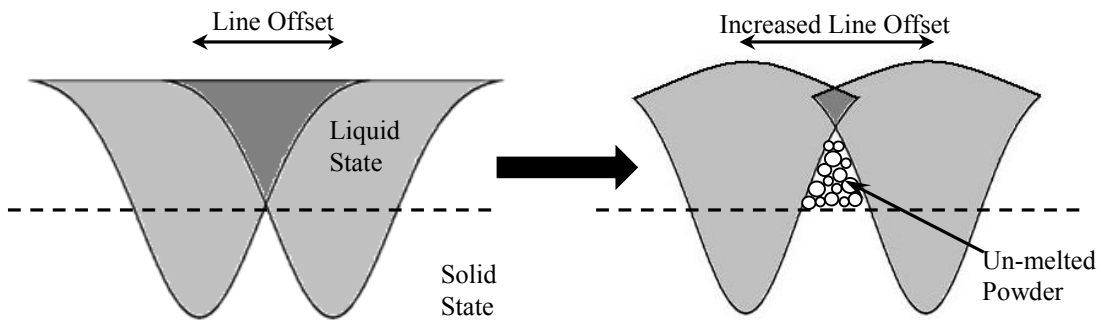


Fig. 15 Schematic of Melt Pool with Increased Line Offset during EBM Process

The porosity is not obvious until the line offset is increased to 0.22mm. Apparent defects are observable on the surface, as shown in Fig. 14 (d). When line offset is increased to 0.26mm and 0.30mm, the melt pool fails to contact the previous hatch line, which leads to bad wetting conditions. In order to reduce total surface free energy, the melted powder easily gathers together and flows above the un-melted powder, causing voids between hatch lines, as shown in Fig. 14 (d)-(f). The un-melted powder is visible through the pores of the top surface. The dual effects of voids and powder gap seriously increase the porosity of specimens made with a large line offset value. According to the solidified surface, it can be inferred that melt pool width is larger than 0.18mm, but less than 0.22mm.

4.2.3 Defects caused by the Increased Focus Offset

Porosity distribution versus focus offset are shown in Fig. 16. The focus offset value does not significantly change the porosity until 16 mA.

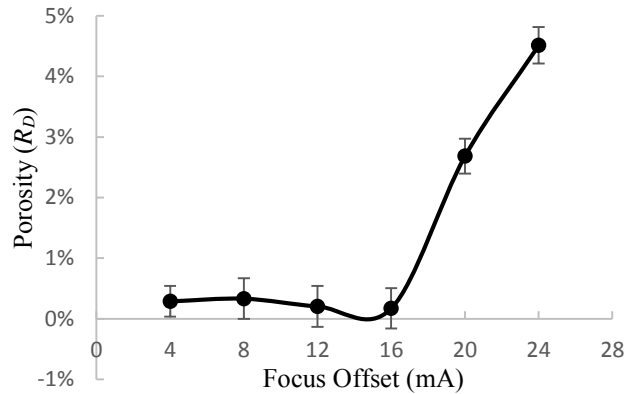


Fig. 16 Porosity versus Focus Offset

Focus offset is the additional current running through the respective electromagnetic coil and can be translated into an offset of the focal plane from its zero position [15]. Increasing the focus offset value results in a larger beam diameter during the EBM process. This can lead to an increased beam spot, but less energy concentration. Thus, energy density is reduced. Solidified surface was also observed under microscope and shown in Fig. 17.

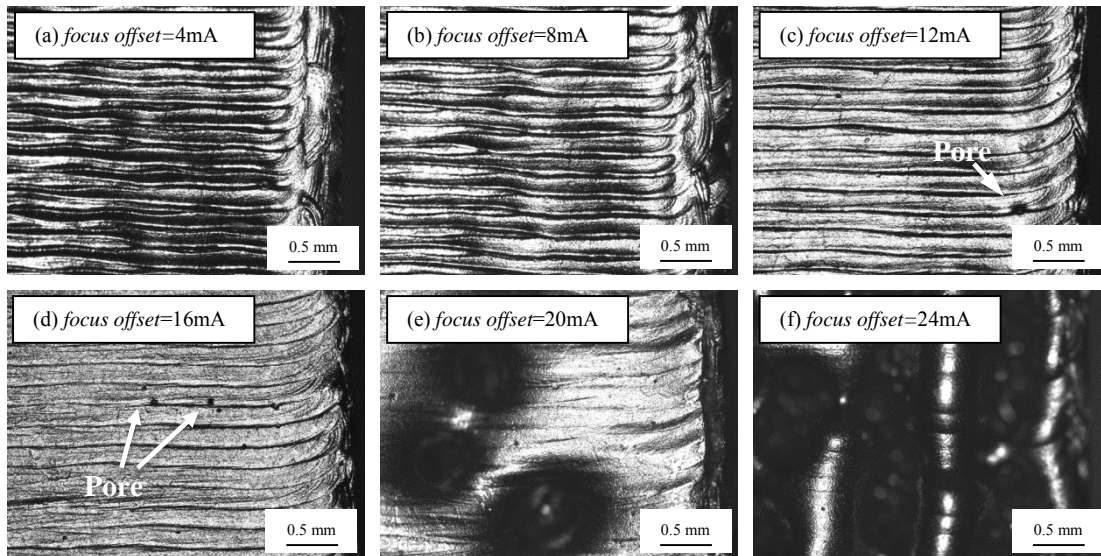


Fig. 17 Solidified Top Surfaces of EBM Specimens by Varying Line Offset

A small focus offset value results in concentrated electron beam spot and profound melting depth. Thus, the penetration depth of an electron beam into the powder layer is greater than that of the laser beam [16]. Previous solidified titanium is also melted to form melt pools which overlap each other to ensure hatching consistency. Each solidified hatch line forms a ridge shape and causes a rough surface. By increasing the focus offset value, the morphology of the melt pool is changed. As shown in Fig. 18, the horizontal melt pool size is enlarged, while the melting depth is reduced.

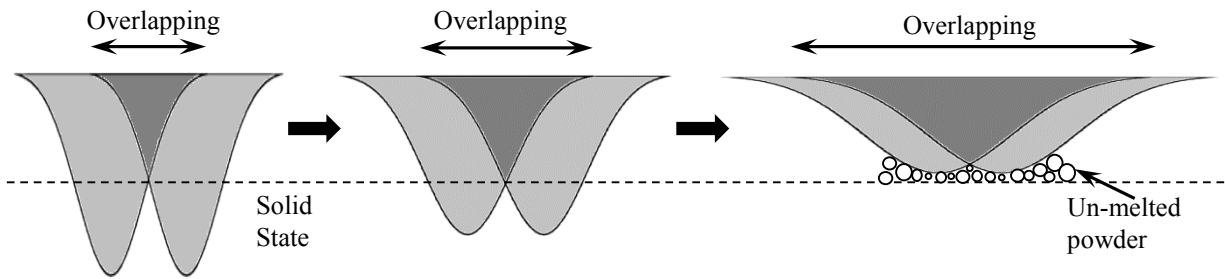


Fig. 18 Schematic of Melting Pool with Increased Focus Offset during EBM Process

Increased overlap area improves the surface roughness significantly as shown in Fig. 17 (c, d). But small pores may be generated at localized areas. These spherical pores result from gaseous argon entrapped in the powder particles caused by the atomization process [8]. The melted powder releases the trapped gas which causes the small defects. However, these defects are barely detectable using the Archimedes method. When focus offset value is higher than 16mA, the increased overlap area and reduced melting depth create an unstable melt pool due to underneath un-melted powder, as shown in Fig. 18. The flowability of molten powder causes interstitial shortage which is reflected by the increased porosity.

4.3 Comparison of Defect Formation between SLM and EBM

Although SLM and EBM are similar in principle, defects are generated in different pattern when deviating processing parameters from optimized parameters. In the SLM process, high energy density causes over melting on the powder bed. The defects are resulted from the blade scraping particles, which are solidified from the ejected molten materials on the surface. Thus, the defects generation is mainly attributed to a physical removal process when using Zone II marginal parameters. By contrast, Arcam EBM system adopts a more complicated feedback control design, compared to EOS system. Higher energy density is hard to be achieved during the EBM process. Generally, no defects could be fabricated even though the electron beam power is increased. Beam current and scanning speed are dynamically controlled to maintain a steady melt pool.

If the input energy fails to melt the metallic powder completely, the defects will be easily formed due to the voids between the remelted materials. In the SLM process, the Zone III defects are attributed to the breaking spots of hatch lines, or gaps between two hatch lines due to the reduced melt pool size. But the increased line offset or focus offset causes the melt pool in an unstable situation in the EBM process, because of the unmelted powder around melt pool. Serious flowability of the molten material results in large voids on the powder bed. Therefore, according to the microscopy, it is anticipated that EBM defects are larger than the SLM defects if energy density is lowered during the melting process.

5. Conclusion

Porosity distribution was investigated by varying processing parameters in this study. The change of processing parameters is directly related to the energy to the Ti-6Al-4V powder bed. Although energy density has a significant effect on defect generation, it is not linearly correlated with porosity. Marginal parameters are responsible for the defect generation during SLM and EBM processes.

In the SLM process, splashed particles are generated by the Zone II marginal parameters and then welded to the top surface. The layer deficiency is caused by the recoater removing the large welded particles. Thus, Zone II marginal parameters indirectly generate defects, which are distributed stochastically in SLM specimens. Defects can be directly formed by Zone III marginal parameters. The insufficient energy density results in voids along or between hatch lines.

For EBM process, the increased line offset and focus offset are similar to the Zone III marginal parameters of SLM. Defects are formed due to insufficient energy density. Interstices between un-melted particles account for a certain amount of porosity in the specimens, while the deteriorated hatch lines exacerbates the inclusion of defects.

Acknowledgements

The authors gratefully acknowledge the support of the Office of Naval Research through awards N00014-09-1-0147 and N00014-10-1-0800, Technical Monitor: Dr. Ignacio Perez. The authors also express their gratitude to the staff of the Rapid Prototyping Center at the University of Louisville for their assistance.

Reference

- [1] W.O. Soboyejo, T.S. Srivatsan. *Advanced Structural Materials: Properties, Design Optimization, and Applications*. CRC Press 2006, 359-400
- [2] J. Hiemenz. Electron beam melting. *Advanced Materials and Processes*. 165(3), 2007, 45-46
- [3] G. Levy, R. Schindel, J.P. Kruth. Rapid manufacturing and rapid tooling with layer manufacturing (LM) technologies, state of the art and future perspectives. *CIRP Annals-Manufacturing Technology*, 52(2), 2003, 589-609
- [4] B. Vandenbroucke, J.P. Kruth. Selective laser melting of biocompatible metals for rapid manufacturing of medical parts. *Rapid Prototyping Journal*, 13(4), 2007, 196-203
- [5] L.E. Murr, S.M. Gaytan, D.A. Ramirez, et al. Metal Fabrication by Additive Manufacturing Using Laser and Electron Beam Melting Technologies. *J. Mater. Sci. Technol.*, 28(1), 2012, 1-14
- [6] L. Facchini, E. Magalini, P. Robotti, et al. Microstructure and mechanical properties of Ti-6Al-4V produced by electron beam melting of pre-alloyed powders. *Rapid Prototyping Journal*, 15(3), 2009, 171-178
- [7] T. Sercombe, N. Jones, R. Day, et al. Heat treatment of Ti-6Al-7Nb components produced by selective laser melting. *Rapid Prototyping Journal*, 14(5), 2008, 300-304
- [8] S. Biamino, A. Penna, U. Ackelid, et al. Electron beam melting of Ti-48Al-2Cr-2Nb alloy: Microstructure and mechanical properties investigation. *Intermetallics*, 19, 2011, 776-781
- [9] M. Kahnert, S. Lutzmann, M. F. Zaeh. Layer Formations in Electron Beam Sintering. *Solid Freeform Fabrication Symposium*, 2007, 88-99

- [10] H. Gong, K. Rafi, T. Starr, et al. Effect of Defects on Fatigue Tests of As-Built Ti-6Al-4V Parts Fabricated By Selective Laser Melting. *Solid Freeform Fabrication Symposium*, 2012, 499-506
- [11] L. Thijs, F. Verhaeghe, T. Craeghs, et al. A study of the microstructural evolution during selective laser melting of Ti-6Al-4V. *Acta Materialia*, 58, 2010, 3303-3312
- [12] A.B. Spierings, M. Schneider. Comparison of density measurement techniques for additive manufactured metallic parts. *Rapid Prototyping Journal*, 17(5), 2011, 380-386
- [13] M. Von Allmen, *Laser-beam Interactions with Materials*, Springer-Verlag, Berlin, 1987. 146-174
- [14] J.P. Kruth, L. Froyen, J. Van Vaerenbergh. Selective laser melting of iron-based powder. *Journal of Materials Processing Technology*, 149, 2004, 616-622
- [15] J. Schwerdtfeger, R. F. Singer, C. Körner. In situ flaw detection by IR-imaging during electron beam melting. *Rapid Prototyping Journal*, 18(4), 2012, 259-263
- [16] M. F. Zaïh, S. Lutzmann. Modelling and simulation of electron beam melting. *Prod. Eng. Res. Devel.* 4, 2010, 15-23